13th World Conference on Earthquake Engineering
Vancouver, B.C., Canada
August 1-6, 2004
Paper No. 662

SIMPLIFIED SHAKING TABLE TEST METHODOLOGY USING EXTREMELY SMALL SCALED MODELS

Noriko TOKUI[1], Yuki SAKAI[2], Yasushi SANADA[3], Naruhito YAMAUCHI[4], Yoshiaki NAKANO[5], Haruhiko SUWADA[6], and Hiroshi FUKUYAMA[7]

SUMMARY

To establish a simple and cost effective testing technique to investigate seismic behaviors of RC structures, extremely small scaled model structures consisting of high performance fiber reinforced cement composite (HPFRCC) material reinforced only with longitudinal reinforcement are fabricated, and their dynamic behaviors are experimentally and analytically investigated.

INTRODUCTION

Shaking table tests have been widely applied to investigate dynamic behaviors of structures under earthquake excitations. In the shaking table tests of reinforced concrete (R/C) structures, relatively large specimens are generally tested to eliminate difficulties in fabricating specimens. However, the number of shaking tables that have enough capacity to carry out large-scale tests are limited, and much cost and time are generally required. Even when shaking table tests using relatively small specimen are carried out, it may be difficult to provide lateral reinforcement in such a scaled specimen. Therefore another methodology is needed to carry out shaking table tests within limited cost.

Recent investigations on high performance fiber reinforced cement composite (HPFRCC) material indicates that tension stiffening as well as multiple cracking effects of HPFRCC may result in ductile behavior. To establish a simple and cost effective testing technique to investigate seismic behaviors of R/C structures, extremely small-scaled column specimens consisting of HPFRCC material reinforced only

[1] Graduate Student, Graduate School of Engineering, University of Tokyo, E-mail: tokui@iis.u-tokyo.ac.jp
[2] Associate Professor, Institute of Engineering Mechanics and Systems, University of Tsukuba, Dr. Eng.
[3] Research Associate, Earthquake Research Institute, University of Tokyo, Dr. Eng.
[4] Technical Associate, Institute of Industrial Science, University of Tokyo
[5] Associate Professor, Institute of Industrial Science, University of Tokyo, Dr. Eng.
[6] Researcher, National Institute for Land and Infrastructure Management, Ministry of Land, Infrastructure and Transport
[7] Chief Researcher, Building Research Institute, Dr. Eng.

with longitudinal reinforcement are fabricated, and their dynamic behaviors are experimentally and analytically investigated.

TEST SPECIMENS

The extremely small-scaled column specimens investigated in this study are not the simply size-reduced models of existing full-scale R/C members but those consisting of longitudinal steel reinforcement and HPFRCC material without lateral reinforcement.

The HPFRCC used in specimens is mortar matrix (water-cement ratio: 45%, sand-cement ratio: 40%) mixed with 1.0% volume ratio of polyethylene fiber (fiber length: 15mm, the diameter of a fiber: 12 μm). Two types of specimens are designed as follows: Type-S (stub) specimen with a stub at each end and Type-P (plate) specimen with a plate at each end. The dimension of specimens is shown in Figure 1. Each specimen has a cross section of 30 x 30 mm and the height *h* of 180 mm. The shear-span-to-depth ratio of each specimen is 3.0, and the tensile reinforcement ratio is 2.19%. For shaking table tests and static loading tests, three Type-S specimens and six Type-P specimens are made. Photo 1 shows a close-up view of casting HPFRCC.

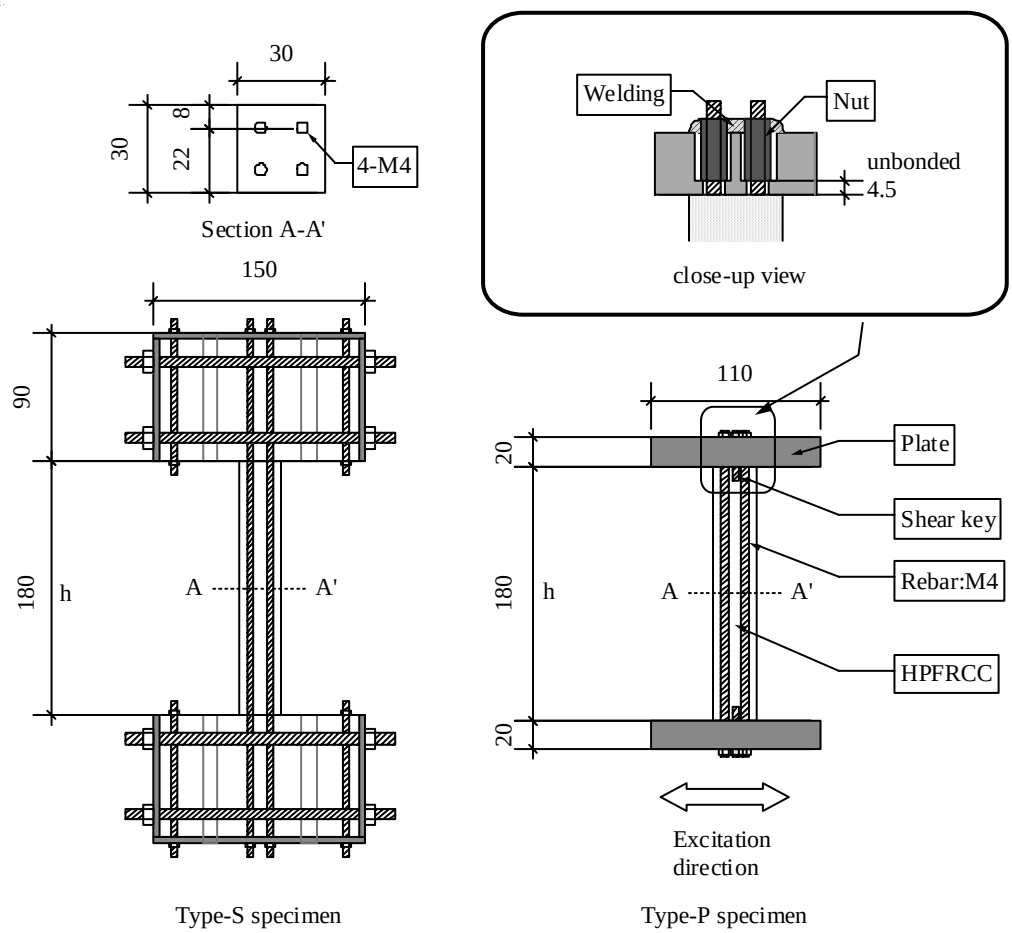

Figure1. Dimension of specimens

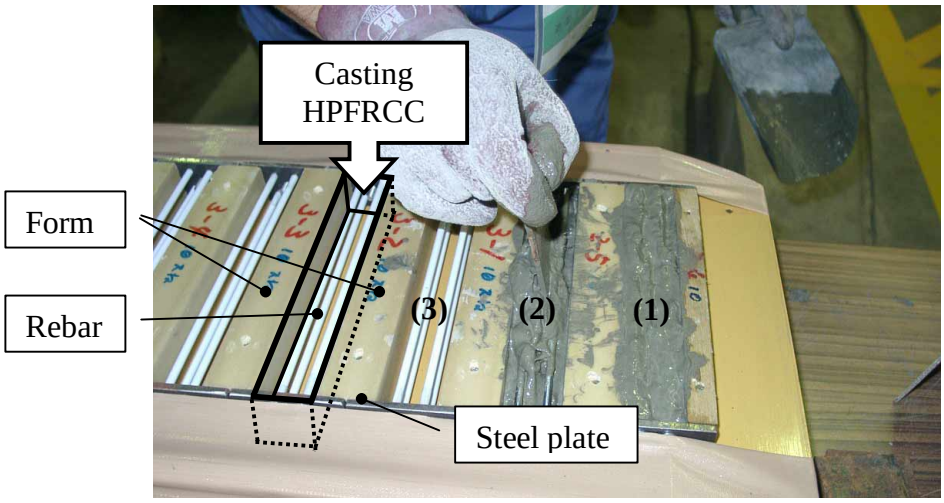

(1) After casting HPFRCC
(2) Under casting HPFRCC
(3) Before casting HPFRCC

Photo 1. Casting HPFRCC

SHAKING TABLE TEST

Test Setup

The loading system is shown in Figure 2. Each specimen is placed on and fixed to component (c). This system has horizontal and vertical sliders, which enables specimens to deform in the lateral and axial direction when they are subjected to anti-symmetric bending during excitations.

The relative displacement y between point (a) and component (c) is measured in the direction of excitation. Accelerometers are installed at point (a), (d), and the shaking table. Load cells (1) and (2) are installed at both ends of the component (c), which is placed on horizontal sliders, to directly evaluate the inertia force acting on the specimen. The inertia force Q of each specimen is calculated from Eqs. (1) and (2) based on the measured force shown in Figure 3.

$$\boldsymbol{Q} - \boldsymbol{P_I} + \left(-\boldsymbol{P_{L1}} - \boldsymbol{P_{L2}} - \boldsymbol{P_{DS}}\right) = 0 \tag{1}$$

Assuming $\boldsymbol{P_{DS}} \approx 0$

$$\boldsymbol{Q} \approx \left(\boldsymbol{P_{L1}} + \boldsymbol{P_{L2}}\right) + \boldsymbol{P_I} \tag{2}$$

$$\boldsymbol{P_I} = \boldsymbol{m} \cdot \boldsymbol{a}$$

where P_{L1} and P_{L2} are the forces measured with load cells (1) and (2), respectively, P_I is the inertia force acting on lower stub and component (c), and m and a are their mass and absolute acceleration, respectively.

To observe the effects of different design details at specimen ends, i.e., stub end and plate end, the rotation angle $\theta_{h'}$ at 10mm above the column base is measured as shown in Figure 4. The data are recorded with a sampling interval of 1/500 sec.

Test Program

In this experiment, the gross weight *W* of a specimen including self-weight and equipment weight is 3234N. The calculated initial period of the specimen is 0.074 seconds. The sine wave of which amplitude increases gradually as shown in Figure 5 is used to excite specimens. The period of the sine wave is 0.20 seconds, which is about 3 times of the calculated period of specimens.

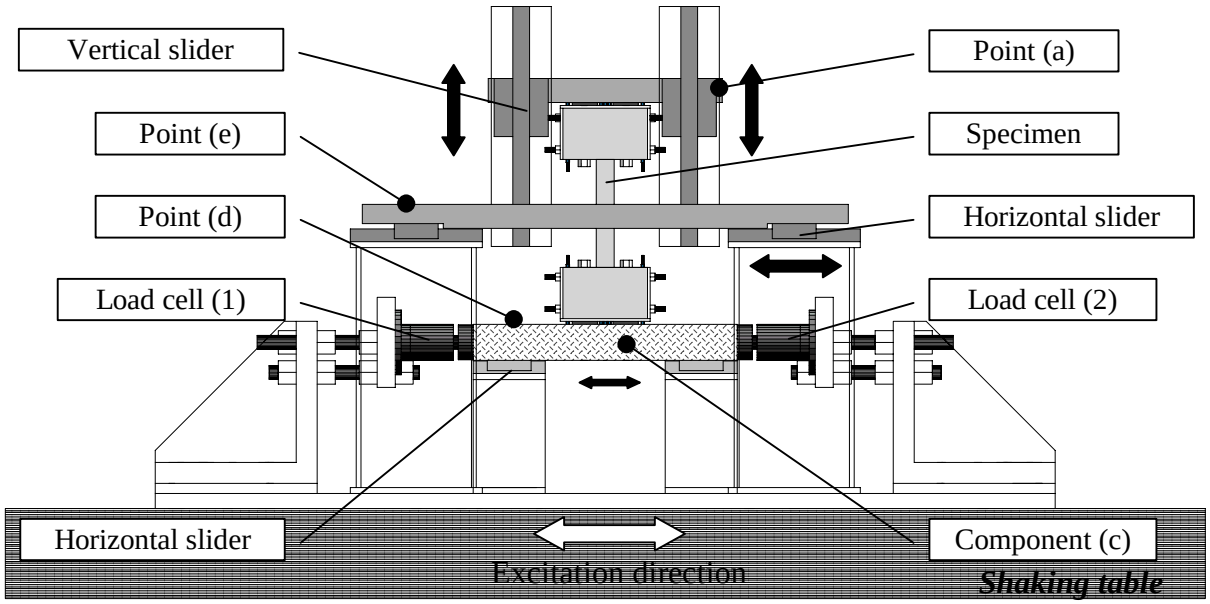

(i) Excitation System

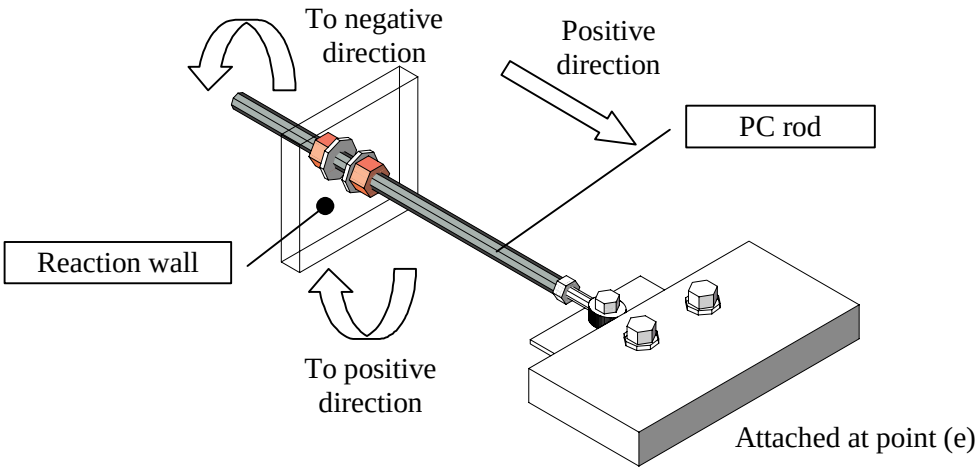

(ii) Static loading equipment attached at point (e)

Figure2. Loading system

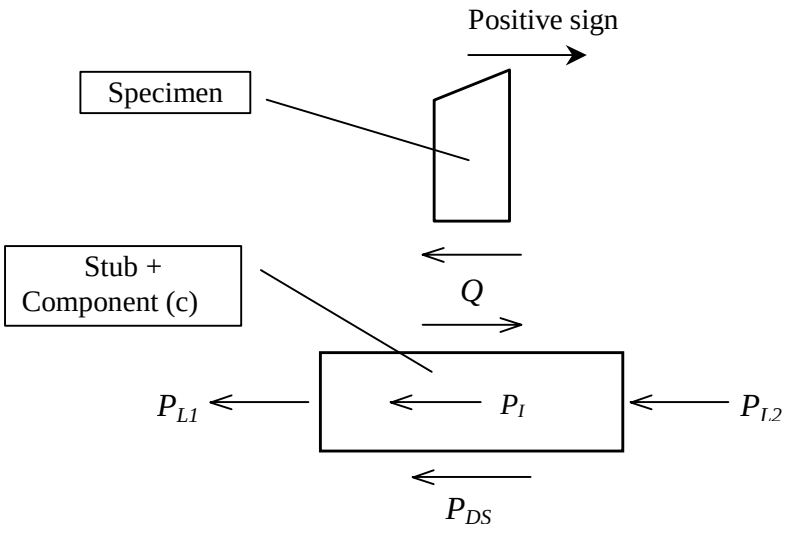

Q: inertia force of specimen
(restoring and damping force)
P_{L1}: force obtained from load cell (1)
P_{L2}: force obtained from load cell (2)
P_I: inertia force of stub and component (c)
P_{DS}: damping force from slider

Figure3. Inertia force of specimen and measured force

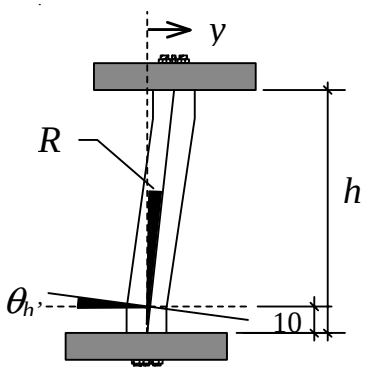

Figure 4.Rotation angle measurement

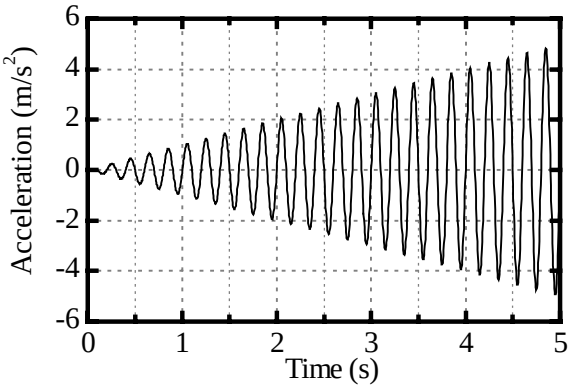

Figure5. Input sine wave

Test Results

Figure 6 shows the relationship of response shear coefficient C (= Q / W) and drift angle R (= y / h) of each specimen. Both specimens show ductile behaviors with spindle shaped hysteretic loops. To compare the fundamental characteristics of extremely small-scaled specimens proposed herein to those of regular R/C members, the following three parameters α_y, β, and h_{eq} are calculated and summarized in Table 1 and Figure7. They are defined as:

(1) α_y: the ratio of secant stiffness at yielding to the initial stiffness.
(2) β: the ratio of post-peak stiffness to the initial stiffness
(3) h_{eq}: equivalent damping factor

The yielding of the specimen is defined as the point where its instant stiffness is lower than 10% of the initial stiffness. As can be found in Table1, these values successfully simulate those of R/C members.

Figure 8 shows the $\theta_{h'}$ - R relationship of both specimens. This figure shows that the ratio of $\theta_{h'}$ of Type-P specimen to that of Type-S specimen lies in the range of 1.5 to 2.0, and the deformation is more significantly concentrated over the end regions for Type-P specimen.

Table 2 shows the maximum Q values (Q_{MAX}) of specimens during shaking table test, together with those of static loading test described later. This Table shows that Q_{MAX} of Type-S specimen is 20% larger than that of Type-P specimen although they have the same sectional and material properties. To understand the reason of different Q_{MAX} values, static loading tests of both specimens are carried out and their fundamental behaviors are carefully investigated.

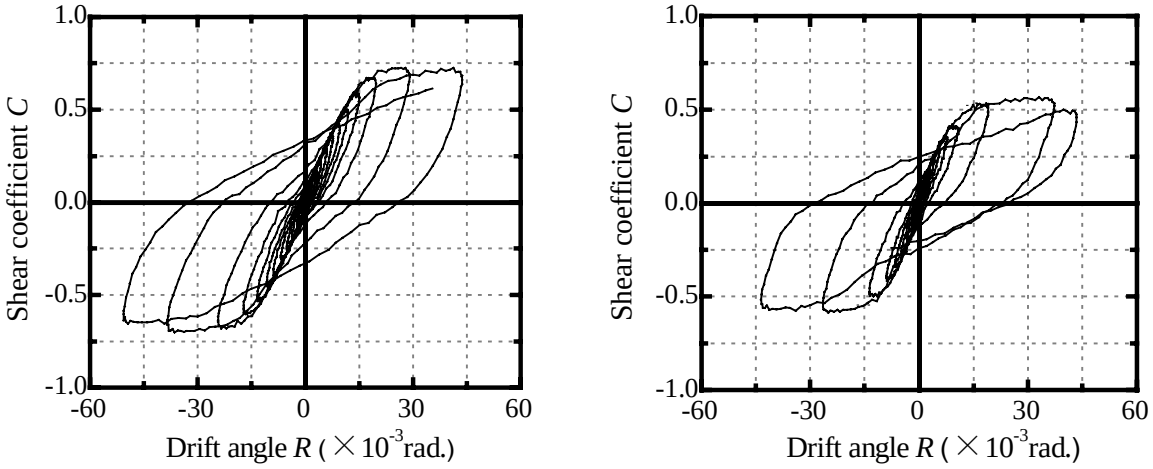

Type-S Type-P

Figure6. Shaking table test results

Table 1. Degradation in stiffness

	α_y	β
Type-S specimen	0.25	0.040
Type-P specimen	0.23	0.033

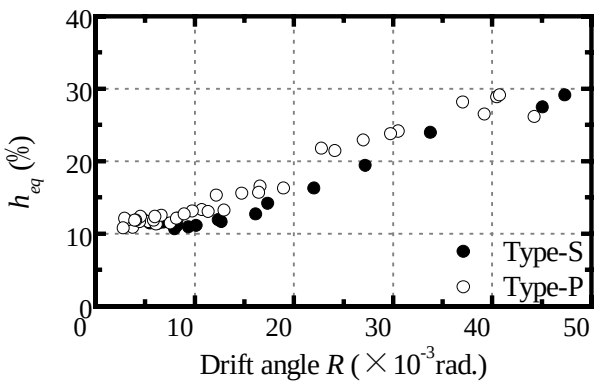

Figure7. Equivalent damping factor

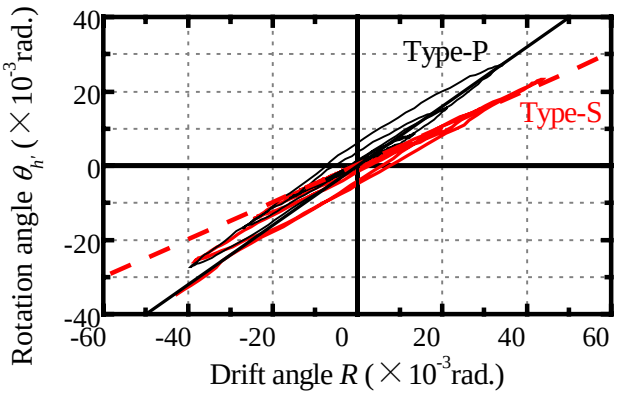

Figure8. $\theta_{h'}$ - R relationship

Table2. Comparison of maximum Q values

	Q_{MAX} (N) [C_{MAX}]		(Shaking Table Test) / (Static Test)
	Shaking Table Test	Static Test	
Type-S specimen	2285 [0.707]	2122 [0.656]	1.08
Type-P specimen	1897 [0.587]	1911 [0.591]	0.99
(Type-S) / (Type-P)	1.20	1.11	

STATIC LOADING TEST

Specimen and Test Setup

The specimens used in static loading tests are the same as those of shaking table tests. For the static tests, the equipment shown in Figure 2 (ii) is attached at the point (e) indicated in Figure 2(i). The displacements obtained in the shaking table tests are applied to each specimen by pushing and pulling point (e). The displacements are imposed with a PC rod by tightening and loosening a nut placed at the reaction wall. After the maximum displacement cycle experienced during the shaking table test is imposed, each specimen is monotonically loaded to collapse.

Test Result

Figure 9 shows the C - R relationship of each specimen. Figure 9 and Table 2 show that the maximum value of C of Type-S specimen is 11% larger than that of Type-P specimen. The higher strength in Type-S specimen may be attributed to the different design details at specimen ends; the Type-S specimen has stub ends where fiber reinforced cement is monolithically cast together with its mid-column part, and the critical sections at both ends can therefore resist tensile actions to some extent even in the post-crack stage, while the Type-P specimen has steel plate ends which do not contribute to the resistance of cracked section.

As can be found in comparison between shaking table test and static loading test shown in Table 2, Q_{MAX} during the shaking table test is 8% higher for Type-S specimen while it is almost same for Type-P specimen. This result implies that the effect of strain rate may be different in Type-S and Type-P specimens.

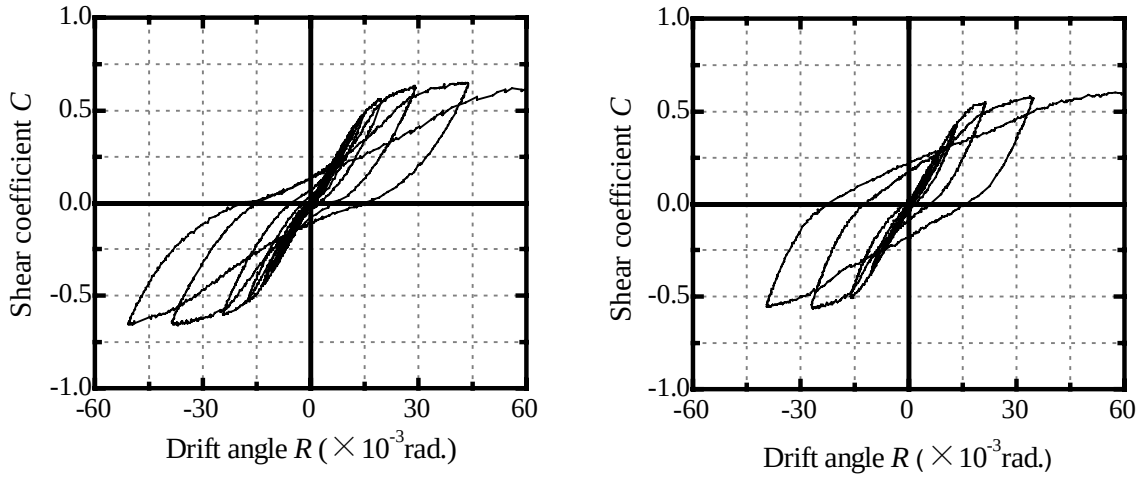

Type-S Type-P

Figure9. Static loading test results

FIBER MODEL ANALYSIS CONSIDERING STRAIN RATE EFFECTS

To investigate the difference in Q_{MAX} due to design details at specimen ends and strain rate effects, fiber model analyses are carried out.

Assumptions in computation

Curvature distributions

Figure 10 shows the curvature distributions assumed in the analysis. As can be found in the figure, a triangular curvature distribution is assumed for Type-S specimens, while a combined profile of rectangular and triangular distribution is assumed for Type-P specimen since the longitudinal reinforcement is unbonded to HPFRCC over the length of h_p in the end plates as shown in Figure 1.

The curvature ${}_s\phi_0$ at the critical section of Type-S specimen at a given displacement ${}_sy$, and the rotation angle ${}_s\theta_{h'}$ at h' (=10 mm) above the column base, is determined by Eqs. (3) and (4), respectively, assuming the curvature distribution shown in Figure 10(a).

$$ {}_s\phi_0 = \frac{3 \cdot {}_s y}{h^2} \tag{3} $$

$$ {}_s\theta_{h'} = \frac{1}{2} {}_s\phi_0 \cdot h' \left(2 - \frac{h'}{h} \right) = \frac{3}{2} \frac{{}_s y}{h} \cdot \frac{h'}{h} \left(2 - \frac{h'}{h} \right) \tag{4} $$

The curvature at the critical section of Type - P specimen, ${}_p\phi_0$, is determined as follows. Based on the curvature distribution of Type-P specimen shown in Figure 10(b), the drift ${}_py$ and the rotation angle ${}_p\theta_{h'}$ at a distance of h' (=10 mm) from the bottom stub are obtained as Eqs. (5) and (6).

$$ {}_P y = \frac{1}{3} {}_p\phi_0 h^2 + {}_p\phi_{hp} \cdot h_p \left(h + \frac{h_p}{2} \right) \tag{5} $$

$$ {}_P\theta_{h'} = \frac{1}{2} {}_p\phi_0 \cdot h' \left(2 - \frac{h'}{h} \right) + {}_p\phi_{hp} \cdot h_p \tag{6} $$

Where ${}_p\phi_0$ and ${}_p\phi_{hp}$ are curvatures at critical section and at h_p below the end plate, respectively. Considering the experimental results shown in Figure 8, the relation of ${}_p\theta_{h'}$ and ${}_s\theta_{h'}$ is assumed as Eq. (7).

$$ {}_P\theta_{h'} = 2\ {}_S\theta_{h'} \tag{7} $$

Setting ${}_py$ of Eq.(5) equal to ${}_sy$ of Eq.(3), the curvature ${}_p\phi_0$ at critical section at a given displacement ${}_py$ (=${}_sy$) is obtained from Eqs. (4) to (7). The location of the neutral axis and the strain of each fiber segment are then determined based on the curvature at critical section ${}_s\phi_0$ (or ${}_p\phi_0$) obtained above, the equilibrium condition of axial force of a section and the plane section assumption.

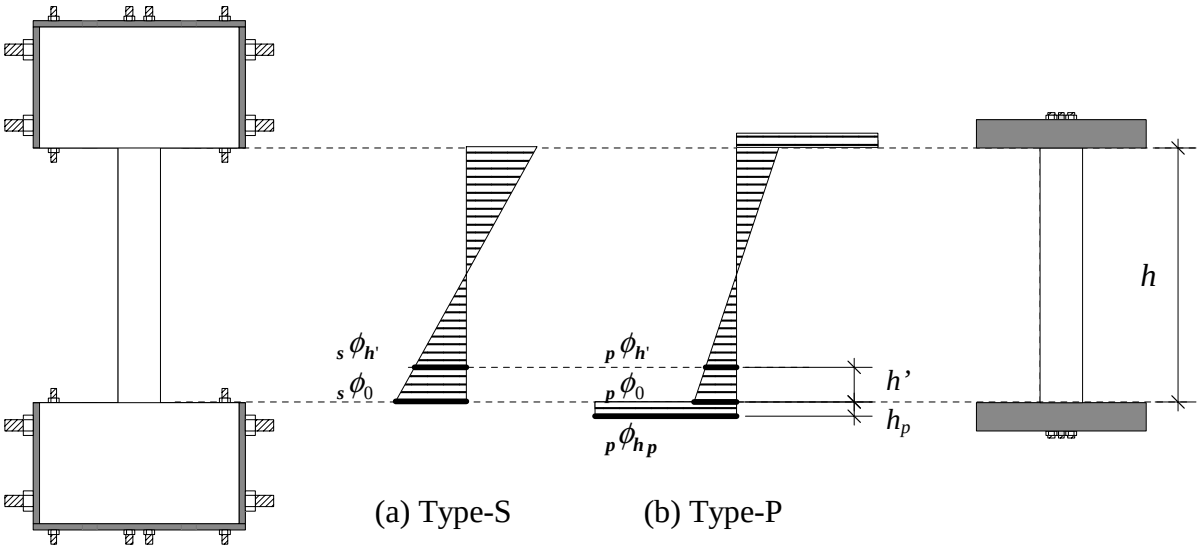

Fig.10 Curvature distribution

Material characteristics

To consider strain rate effects on the σ - ε relationship on material characteristics basis, the strain rate ${}_k\dot{\varepsilon}$ is calculated by Eq. (8).

$$ {}_k\dot{\varepsilon} = \Delta_k \varepsilon / \Delta t \tag{8} $$

Where $\Delta_k\varepsilon$ and Δt are the strain increment of element k and the time increment, respectively.

Tables 3 and 4 show the mechanical properties of HPFRCC and longitudinal reinforcement obtained by the static material tests. Figure 11 shows material properties model for HPFRCC and longitudinal reinforcement.

In compression, the σ - ε relation of HPFRCC is represented with (1) a linear line having a slope of initial Young's modulus E_c, (2) a parabola curve that passes through the origin (0, 0) and the peak (ε_B, σ_B), (3) a linearly falling branch and (4) a residual strength plateau with $0.5\sigma_B$. In tension, a tensile strength of $\sigma_B/20$ after yielding is assumed up to 2% for Type-S specimen, while the strength contribution is neglected for Type-P specimen. The Young's modulus E_c and strength σ_B shown in Table 3 is factored in accordance with strain rate, as shown in Eqs. (9) through (12).

In both tension and compression, the σ - ε relation of longitudinal reinforcement is represented with (1) a linear line having initial Young's modulus *Es* and (2) a linear line with 1/100 E_s. The yield strength σ_y show in Table 4 is factored in accordance with strain rate, as shown in Eq. (13).

HPFRCC

Young's modulus

$$\begin{aligned} &|\dot{\varepsilon}| > 10^1 \mu/\sec \\ &\qquad {}_d\boldsymbol{E_c} = \left(0.02 \cdot \log|\dot{\varepsilon}| + 0.98\right) \cdot {}_s\boldsymbol{E_c} \\ &|\dot{\varepsilon}| \le 10^1 \mu/\sec \\ &\qquad {}_d\boldsymbol{E_c} = {}_s\boldsymbol{E_c} \end{aligned} \tag{9}$$

Where, ${}_d\boldsymbol{E_c}$: Young's modulus of HPFRCC (dynamic)

${}_s\boldsymbol{E_c}$: Young's modulus of HPFRCC (static)

Compressive strength

$$\begin{aligned} &|\dot{\varepsilon}| > 10^1 \mu/\sec \\ &\qquad {}_d\sigma_B = \left(0.06 \cdot \log|\dot{\varepsilon}| + 0.94\right) \cdot {}_s\sigma_B \\ &|\dot{\varepsilon}| \le 10^1 \mu/\sec \\ &\qquad {}_d\sigma_B = {}_s\sigma_B \end{aligned} \tag{10}$$

Where, ${}_d\sigma_B$: Compressive strength of HPFRCC (dynamic)

${}_s\sigma_B$: Compressive strength of HPFRCC (static)

Tensile strength

・Type-S

$$\sigma_t = \sigma_B / 20 \quad (\sigma_B = {}_s\sigma_B \text{ or } {}_d\sigma_B) \tag{11}$$

・Type-P

$$\sigma_t = 0 \tag{12}$$

Longitudinal reinforcement

Yield strength of longitudinal reinforcement

$$\begin{aligned} &|\dot{\varepsilon}| > 10^2 \mu/\sec \\ &\qquad {}_d\boldsymbol{f_y} = \left(0.05 \cdot \log|\dot{\varepsilon}| + 0.90\right) \cdot {}_s\boldsymbol{f_y} \\ &|\dot{\varepsilon}| \le 10^2 \mu/\sec \\ &\qquad {}_d\boldsymbol{f_y} = {}_s\boldsymbol{f_y} \end{aligned} \tag{13}$$

Where, ${}_d\boldsymbol{f_y}$: Yield strength of longitudinal reinforcement (dynamic)

${}_s\boldsymbol{f_y}$: Yield strength of longitudinal reinforcement (static)

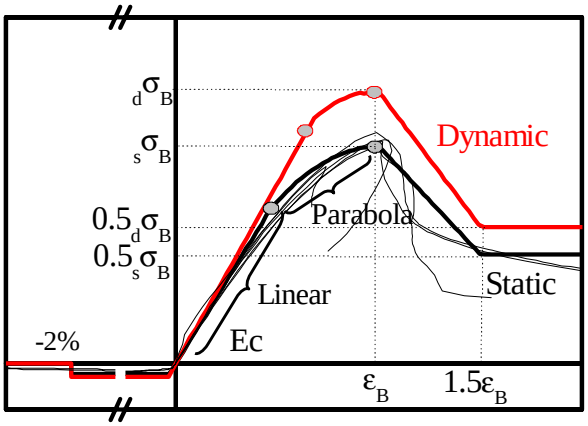

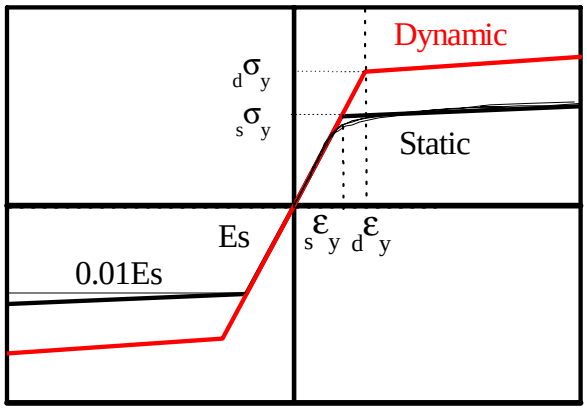

$_s\sigma_B = 47(N/mm^2)$, $_s\varepsilon_B = 0.4(\%)$

$E_c = 1.8\times10^4(N/mm^2)$

HPFRCC

$_s\sigma_y = 450(N/mm^2)$

$E_s = 1.35\times10^5(N/mm^2)$

Longitudinal Reinforcement

Figure11. Model of material properties

Table3. Mechanical Properties of HPFRCC (obtained from static material test)

Loading pattern	Specimen	Age (days)	Young's modulus*1 E_c (N/mm^2)	Compressive strength σ_B (N/mm^2)	Strain at compressive strength ε_B (%)	Tensile strength σ_t (N/mm^2)
Dynamic	S10M (Type-S)	19	1.95×10^4	45.74	0.34	2.00
	P10M (Type-P)	18	1.69×10^4	47.68	0.40	2.14
Static	S10M (Type-S)	16	1.75×10^4	48.74	0.42	-*3
	P10M (Type-P)	18	1.69×10^4	47.68	0.40	2.14

*1 secant modulus at 1/3 σ_B
*2 average of 3 cylinders
*3 not measured

Table4. Mechanical Properties of Longitudinal reinforcement (obtained from static material test)

	Section area (mm^2)	Young's Modulus E_s (N/mm^2)	Yield strength *1 σ_y (N/mm^2)	Yield strain ε_y (%)
M4	9.87	1.35×10^5	443.77	0.55

*1 0.2% off-set value
*2 average of 3 test pieces

Results and Discussions

Computed results are compared with static loading test results in Figure 12 and shaking table test results in Figure 13, respectively. Figure 14 shows the strain rate and its corresponding magnification factor of tensile reinforcement at the critical section of each specimen obtained in the computation.

As is found in Figure 12, Q_{MAX} can be predicted considering the contribution of fiber reinforced cement composite material to tension resistance in Type-S specimen and neglecting such contribution in Type-P specimen.

The computed Q_{MAX} of Type-S specimen subjected to dynamic loading agrees well with the test result considering the strain rate effects. The strain rate and corresponding magnification factor of material strength is, as shown in Figure 14, generally lower in Type-P specimen, which is attributed to a curvature profile different from that assumed for Type-S specimen. Although the computed Q_{MAX} of Type-P specimen is accordingly lower than that of Type-S specimen, it is still higher by 15% than experimental results.

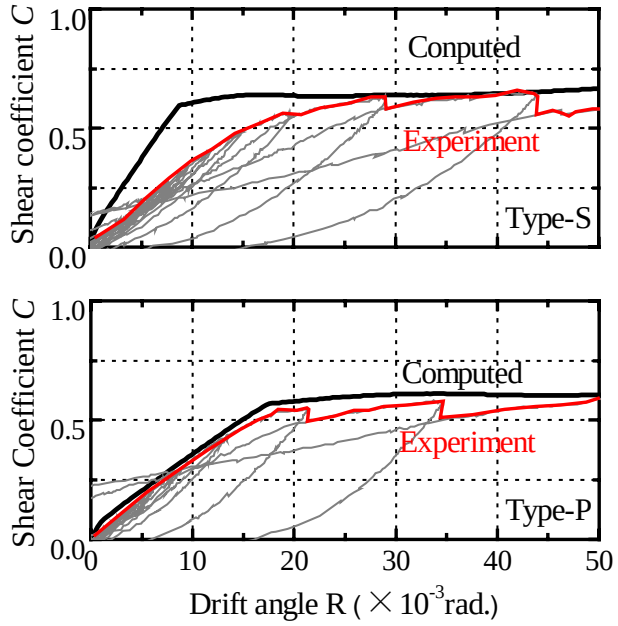

Figure12. Comparison of computed results with static test result

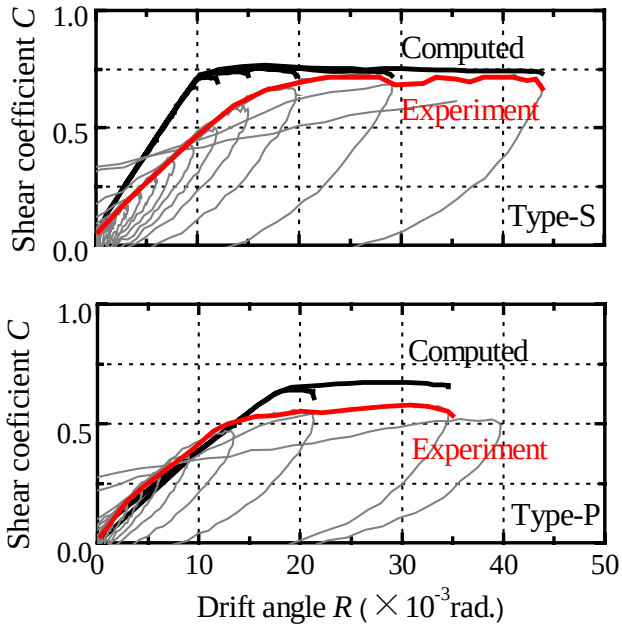

Figure13. Comparison of computed results with dynamic test result

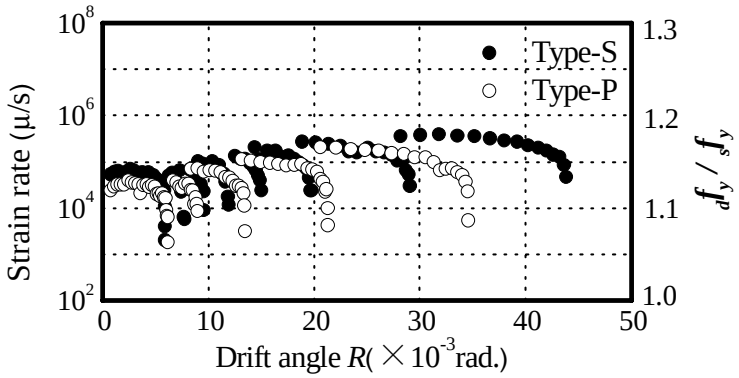

Figure14. Computed strain rate of tensile reinforcement

CONCLUSION

To establish a simple and cost effective testing technique to simulate seismic behaviors of R/C structures, extremely small-scaled model structures consisting of high performance fiber reinforced cement composite (HPFRCC) material reinforced only with longitudinal reinforcement are fabricated, and their behaviors are experimentally and analytically investigated.

1) The specimens of fabricated and investigated in this study can simulate the behavior of actual R/C members.
2) Q_{MAX} under static loading can be predicted considering the contribution of fiber reinforced cement composite material to tension resistance in Type-S specimen and neglecting such contribution in Type-P specimen.
3) The computed Q_{MAX} of Type-S specimen subjected to dynamic loading agrees well with the test result considering the strain rate effects. Although the computed Q_{MAX} of Type-P specimen is lower than that of Type-S specimen, it is still higher by 15% than experimental results.

REFERENCES

1. High Performance Fiber Reinforced Cement Composites (HPFRCC 2), A. E. Naaman and H. W. Reinhardt Ed., RILEM Proceeding 31, 1995
2. Kanda, T.: Material Design Technology for High Performance Fiber Reinforced Cementitious Composite, Concrete Journal, Vol. 38, No. 6, pp. 9-16, Jun., 2000
3. Sato, Y. Fukuyama, H. Suwada, H.: A Proposal of Tension-Compression Cyclic Loading Test Method for Ductile Cementitious Composite Materials, Journal of Structural and Construction Engineering, No.539, pp. 7-12, Jan., 2001
4. Hiroshi, H. Tuneo, O. Yoshikazu, K. Yoshiaki, N. Fumitoshi, K.: Fiber Model Analysis of Reinforced Concrete Members with Consideration of The Strain Rate Effect, Journal of Structural and Construction Engineering, No.482, pp. 83-92, Apr., 1996

ACKNOWLEDGEMENTS

The authors gratefully acknowledge Dr. K. Fujii, Postdoctoral Research Fellow at the Institute of Industrial Science, the university of Toyo, for his enthusiastic contribution to preparing this report. The Central Workshop at the Institute of Industrial Science is also greatly appreciated for its technical support in fabricating specimens.